Decay Dynamics of the Predissociating High Rydberg States of NO

F. Remacle*

Département de Chimie, B6, Université de Liège, B 4000 Liège, Belgium

Marc J. J. Vrakking

FOM Institute for Atomic and Molecular Physics, Kruislaan 407, 1098 SJ Amsterdam, The Netherlands

Received: April 29, 1998; In Final Form: July 1, 1998

The dynamics of predissociating high molecular Rydberg states of NO below the lowest ionization threshold is computed in the presence of a weak external dc field using a quantum theory based on an effective Hamiltonian formalism. The core−electron interaction affecting the low l states ($l \leq 2$) is taken into account by molecular quantum defect theory, while for the high l states ($l \geq 2$), a long range multipolar expansion is used to describe the effect of the anisotropy of the molecular core. Time- and frequency-resolved ZEKE spectra are computed. In the energy range investigated, the decay kinetics of the ZEKE intensity is found to exhibit two time scales, which differ by more than an order of magnitude. The short decay constant typically falls in the submicrosecond range and is in agreement with previous experimental results and computations. In addition, our computations predict a long-time component, which decays in the tens of microseconds range. The two decay times are discussed in terms of the short and long range interseries dynamics, in terms of the strength of the external dc field, and in terms of the nature of the bottlenecks in phase space for a predissociating molecular core with a rather large rotational constant ($B_{NO^+} = 1.9842$ cm^{-1}). It is found that for this particular case where all series are coupled to the fragmentation channels through a low l bottleneck, the predissociation process does not quench the long time component in the decay kinetics. The reason is that the interplay between the interseries coupling and the external dc field leads to a shift of the decay constants to larger values together with an enhancement of the weight of the long time component in the decay kinetics. Special attention is devoted to the role of the dipolar interaction and its synergy with the external dc field.

1. Introduction

ZEKE (zero electron kinetic energy) spectroscopy[1−11] has provided valuable insight into the dynamics of high atomic and molecular Rydberg states.[12−24] In ZEKE spectroscopy, the lifetimes of high Rydberg states have been found to be orders of magnitude longer than what was expected by extrapolating the lifetimes at low n using an n^3 scaling law and extremely sensitive to external perturbations such as an external dc field, an external magnetic field, or the presence of neighboring ions. The role of the external dc field in diluting the coupling strength to the decay channels over the entire l manifold and increasing the lifetime was early on pointed out by Bordas[25] and Chupka[26,27] and then studied in more detail.[28−37] The lifetimes of high molecular Rydberg states are also considerably enhanced by collisional effects and the presence of a magnetic field.[3,15,18,38−44] Moreover, experimentally, the decay kinetics of the ZEKE intensity very often exhibits a bimodal character,[17,45,46] with a prompt and a delayed component. This bimodal decay of the ZEKE intensity was also recovered theoretically both from a kinetic model[47] and from dynamical computations.[48−51]

For large molecules, it was argued early on[45] that the interseries coupling induced by the anisotropy of the molecular core plays an important role in stabilizing high molecular Rydberg states by trapping the Rydberg electron in excited states of the molecular core where it is not directly coupled to the ionization continua. Classical[30,52] and quantum dynamical computations[48,49] showed that for a molecular core with a low rotational constant ($B \leq 0.1$ cm^{-1}) excited above the lowest ionization threshold, the interseries coupling in synergy with the external dc field can act to stabilize the Rydberg states.

The purpose of our current study is to explore the dynamics of predissociating high Rydberg states of NO excited below the lowest ionization threshold where predissociation is the only dissipative mechanism energetically allowed. There have been many experimental[12,53−59] and theoretical[60−62] studies of the Rydberg states of NO previously, which makes this a "benchmark" molecule. In the molecular Hamiltonian, we take into account the effect of the external dc field and the effect of the molecular anisotropy of NO^+. For the latter, both short range (in the sense that they affect low l Rydberg states, which are localized close to the molecular core) and long range core−electron interactions (affecting high l Rydberg states localized far from the core) are included together for the first time. The core−electron interaction among penetrating orbitals ($l \leq 2$) is accounted for by using MQDT theory[63−65] (in a way similar to previous studies[37,62]) and the long range one among nonpenetrating orbitals ($l > 2$) is described by a multipolar expansion,[48,66,67] where we retain the dipolar and the quadrupolar terms. We use an effective Hamiltonian formalism[68,69] to take into account the predissociation process. We compute the

* Corresponding author. Chercheur Qualifié, FNRS, Belgium. Fax: 32 4 3663413. E-mail: fremacle@ulg.ac.be.

10.1021/jp982053x CCC: $15.00
Published on Web 09/15/1998

dynamics via the diagonalization of the effective Hamiltonian as in previous theoretical studies.[37,48,61,62,70−72] We note that when only core−electron interactions among low l states are taken into account, it is also possible to incorporate the effect of the external dc field in the MQDT formalism[73−75] and an extension to higher molecular Rydberg states has recently been published.[76]

A key question to be answered by our study is whether interseries coupling to Rydberg series converging on higher rotational states of the NO^+ core is a mechanism that leads to trapping and the occurrence of an additional long-time component, as in earlier studies,[30,45,48,52,77] or is more important as an additional decay channel, which quenches the long lifetimes. Compared to the earlier theoretical work on NO,[61,62] we have extended the treatment to higher electric field strengths in order to assess the importance of electric fields and interseries coupling under typical ZEKE conditions. At excitation energies just below the lowest ionization threshold, these conditions usually imply that one or more series converging on the rotational levels of the core are beyond the Inglis−Teller (IT) limit ($F_{IT} \geq 1/(3n^5)$).[78] In such a case, the computational results presented below will show that in addition to the short range core−electron interactions affecting predominantly the low l states, it is also important for the dynamics to include the long range interseries coupling terms among higher l states. The computations reported in this study are done at the energy of $n \approx 100$ in the lowest Rydberg series $N^+ = 0$ in the presence of an external dc field. As a result of their multiseries character (isoenergetic Rydberg states belonging up to as many as five different rotational states of the NO^+ core are included in the basis sets) and of the intraseries l and n mixing induced by the external dc field, the size of the basis sets becomes rapidly prohibitive as n increases and it is not possible for us to repeat them at $n \approx 200$ (where ZEKE experiments are usually performed). However, by moving to higher strengths of the field, we expect that our conclusions about the interplay between the short and long range interseries coupling and the intraseries coupling due to the external dc field can provide useful insight about the dynamics in the range of n values, i.e., $n \approx 200$, where many series are above the IT limit, even for extremely small values of the stray field.

As we will show, the decay kinetics of the computed ZEKE intensity can accurately be fitted to a biexponential form leading to the determination of two time scales, a short one in the submicrosecond range and a much longer one in the tens of microseconds. The presence of a short- and a long-time component in the decay kinetics is typical of a dense manifold of quasibound states, coupled to a small number of product channels,[79] as is the case of high molecular Rydberg states[72] (see sections 2 and 3). The short decay time is in agreement with the previous experimental[55] and computed results.[61,62] In addition, we predict the existence of a *much longer* time scale in the decay. As is discussed below, this long-time component is due to a synergy between the interseries coupling and the external dc field, which leads to a lengthening of the lifetimes and a better accessibility of the long-living states, despite the fast zero-order predissociating rates of the low l states of the higher rotational states of the core.

An important conclusion of our work is that in NO in the presence of external dc fields just below or beyond the Inglis−Teller limit, the inclusion of the interseries coupling does not shorten the lifetimes. This would certainly be the case if the interseries coupling were taking place predominantly among low l states. Rather, our computational results (discussed in section 3) show that through the dipolar interaction, a large part of the interseries coupling takes place among high l Rydberg states belonging to adjacent rotational states of the molecular core (states for which $\Delta N^+ = \pm 1$). This interseries mixing is assisted by the intraseries mixing induced by the external dc field. As a result, the long-time component of the ZEKE intensity, which is almost absent in the one series computation, is considerably enhanced when the interseries coupling is included.

We have previously studied in detail[48,49] the decay dynamics of the high molecular Rydberg states of the sodium dimer Na_2 excited above the lowest threshold for ionization. The phase space of high molecular Rydberg states of NO below the lowest ionization threshold differs from that of Na_2 above the lowest threshold for ionization in two fundamental aspects. The first one is that in the case of Na_2^+, no predissociation of the molecular core was allowed and the only dissipative mechanism for the decay of the ZEKE intensity was the rotational autoionization of the high molecular Rydberg states. In this case, the gateway to the ionization continua is localized in the low l Rydberg states built on the lowest rotational state of the molecular core that are isoenergetic with the continuum and coupled to the states initially excited. There is, therefore, a narrow bottleneck to the exit channels, localized in a *single* series, since the Rydberg states built on higher rotational states of the core are not directly coupled to the continua. On the other hand, the low l Rydberg states of NO can predissociate, and for excitation energies below the lowest ionization threshold, this is the only mechanism for dissipation. In the case of a predissociation process, there is a bottleneck to the fragmentation channels in the low l states of *each* series. As the rotational quantum number increases, the rate for predissociation increases too (since for a given excitation energy, higher states of the core mean lower values on the principal quantum number of the electron, n, and the predissociation widths scale as $1/n^3$ at zero order). The structure of the bottlenecks for predissociation in the case of NO below the lowest ionization threshold is therefore different from that of the bottleneck for ionization in the case of Na_2. The second important difference between the two molecules is the value of the rotational constant B; $B_{NO^+} = 1.9842\ cm^{-1}$, while $B_{Na_2^+} = 0.1\ cm^{-1}$. The density of Rydberg states in neighboring series coupled by the molecular anisotropy is much higher in the case of a molecular core with a low rotational constant, i.e., smaller than $0.1\ cm^{-1}$, than for cores with a rotational constant in the range of a few wavenumbers, like that of NO^+. The sparser density of isoenergetic states in NO^+ together with the structure of the bottlenecks characteristic of a predissociation process formed the motivation for the current work and has important consequences for the dynamics that are discussed in sections 3 and 4. The molecular Hamiltonian is described in section 2 together with a brief summary of the formalism used to compute the ZEKE cross section (which is described in detail in ref 80). The cylindrical symmetry is preserved in the presence of an external dc field, and the symmetry-breaking interactions induced by the presence of surrounding ions are not included in the Hamiltonian. Qualitatively, the symmetry-breaking interactions of high Rydberg states with neighboring ions are responsible for the mixing between the high m states, which are better shielded from the molecular core since $l \geq m$ and therefore almost stable, and the low m Rydberg states, which interact better with the core and decay faster. As a result, the effect of the interactions with surrounding ions is to lead to a further enhancement of the lifetimes. The inclusion of such effects in the formalism leads

to even larger basis sets, which are, at the present stage, prohibitive from a computational point of view.

2. Details of the Computations

2.1. Molecular Hamiltonian. The Hamiltonian describes a Rydberg electron interacting with a rotating singly charged anisotropic core in the presence of the external dc field:

$$H = H_{\text{elec}} + H_{\text{rot}} + V + U$$

$$H_{\text{elec}} = \mathbf{p}^2/2 - 1/\mathbf{r}, \quad H_{\text{rot}} = BN^+(N^+ + 1) \qquad (2.1)$$

$$U = \mathbf{r}\cdot\mathbf{F}$$

In eq 2.1, the Hamiltonian is written in atomic units, the vector $\mathbf{r}$ is the distance to the core, B is the rotational constant, and N^+ the rotational angular momentum of the molecular core NO^+. $\mathbf{F}$ is the electrical field, which is taken to be in the z direction and serves as the quantization axis for the spaced fixed basis set. V describes the core−electron interactions and is discussed below. The model Hamiltonian (2.1) is valid for an isolated molecule in a cylindrical symmetric external field. It cannot therefore be used to describe the effect of a finite ion density surrounding the molecule.[3,18,38,40,44] The projection quantum number, M, of the total angular momentum excluding spin, $\mathbf{N} = \mathbf{N}^+ + \mathbf{l}$, is conserved. Consequently, in the computations, the basis set is reduced to a subspace of a given value of M.

To describe the core−electron interactions V, we distinguish between low l Rydberg electrons, which penetrate significantly into the core region and experience strong short range interactions (with valence electrons and with the nuclei), and the high l Rydberg electrons, $l > 2$, which do not penetrate significantly into the core region. We use the formalism of MQDT[63−65] at short range (i.e., for $l \leq 2$) as was done previously[37,62] and a long range multipolar expansion at large core−electron separations, $\mathbf{r}$ (i.e., for $l > 2$).

The MQDT formalism leads to a parametrization of the core−electron interaction by quantum defects affecting low l Rydberg electrons ($l \leq 2$). When the electron is close to the core, it has a higher velocity than the vibrational and rotational motions and therefore adjusts to the motions of the core (Born−Oppenheimer regime). The orbital angular momentum l of the Rydberg electron is strongly coupled to the internuclear axis with a projection Λ and combines with the rotational angular momentum of the molecule $\mathbf{R}$ to yield the total angular momentum excluding spin $\mathbf{N} = \mathbf{L} + \mathbf{R}$. This situation corresponds to Hund case (b) coupling scheme,[81] and the good zero-order quantum numbers are l, N, and Λ. On the other hand, at long range, the electron moves much more slowly than the vibrational and rotational motions of the core. Then, it is better described in a spaced fixed rather than in a molecular fixed basis set, which for a rotating core corresponds to Hund's case (d). The good zero-order quantum numbers in the Hund's case (d) coupling scheme are l, N, and N^+, and the total angular momentum excluding spin is given by $\mathbf{N} = \mathbf{L} + \mathbf{N}^+$. This situation where the electron moves much more slowly than the nuclei can be described as an inverse Born−Oppenheimer regime[82] where the electron moves in the potential generated by the fast motion of the nuclei.

The MQDT electronic Hamiltonian for the low l states is nearly diagonal in Hund's case (b), except for a few terms that describe the mixing of $s\sigma$ and $d\sigma$ configurations. In the Hund case (b) basis set, the diagonal elements of the Hamiltonian are

$$H^{(\text{b})}_{\text{elec}}[lN\Lambda, lN\Lambda] = -\mu_{l\Lambda}/\nu^3 \qquad (2.2)$$

where $\mu_{l\Lambda}$ is the quantum defect due to the core−electron interaction and ν is the effective principal quantum number of the Rydberg state. As a result of the mixing between the $s\sigma$ and $d\sigma$ configurations, the s and $d\sigma$ states must be modified as follows:[60]

$$H^{(\text{b})}_{\text{elec}}[sN0,sN0] = -(\mu_{s\sigma}\cos^2\theta + \mu_{d\sigma}\sin^2\theta)/\nu_{s\sigma}^{3/2}\nu_{d\sigma}^{3/2}$$

$$H^{(\text{b})}_{\text{elec}}[dN0,dN0] = -(\mu_{s\sigma}\sin^2\theta + \mu_{d\sigma}\cos^2\theta)/\nu_{s\sigma}^{3/2}\nu_{d\sigma}^{3/2} \qquad (2.3)$$

and a nondiagonal sd term must be included

$$H^{(\text{b})}_{\text{elec}}[sN0,dN0] = -\frac{1}{2}\sin 2\theta(\mu_{s\sigma} - \mu_{d\sigma})/\nu_{s\sigma}^{3/2}\nu_{d\sigma}^{3/2} \qquad (2.4)$$

In the case of NO, the mixing angle θ was determined to be 38.7°.

Neither the Hund's case (b) basis set, which corresponds to a Born−Oppenheimer description, nor the Hund's (d) basis set, which corresponds to an inverse Born−Oppenheimer situation, leads to a diagonal molecular Hamiltonian. In the Hund's case (b) basis set, the electronic Hamiltonian is almost diagonal but the rotational part takes a complicated form. On the other hand, in the Hund's case (d) basis set, the rotational part is diagonal and the effect of the external electrical dc field is more readily included (for a recent treatment of the effect of an external dc field using a MQDT formalism, however, see ref 76.) Moreover, it has been shown for a model Hamiltonian solvable analytically[82] that in the regime of high n Rydberg states, the diabatic inverse Born−Oppenheimer basis set, here Hund's case (d), is the most appropriate zero order description. We will, therefore, as in previous studies,[61,62] build the matrix of the Hamiltonian in the Hund's case (d) basis set. This zero-order basis set, where the electron is decoupled from the core, can be thought of as the "natural" basis set for high n Rydberg states, since a high n Rydberg electron is for the major fraction of the electronic period far from the molecular core in a well-defined rotational state.

For low l states, $l \leq 2$, the electronic Hamiltonian including the core−electron interaction as parametrized by the MQDT theory is initially written in the Hund case (b) basis set (eqs 2.2−2.4). It is transformed to the Hund's case (d) basis using a frame transformation:[64,83−85]

$$H^{(\text{d})}_{\text{elec}}[lNN^+,l'NN^{+\prime}] = \sum_{\Lambda\Lambda'} A_{N^+\Lambda} H^{(\text{b})}_{\text{elec}}[lN\Lambda,l'N\Lambda'] A_{N^{+\prime}\Lambda'} \qquad (2.5)$$

with

$$A_{N^+\Lambda} = (-1)^{l+\Lambda-N^+}\begin{pmatrix} l & N & N^+ \\ -\Lambda & \Lambda & 0 \end{pmatrix}(2N^+ + 1)^{1/2}[2/((1 + \delta_{\Lambda 0})]^{1/2} \qquad (2.6)$$

where $H^{(\text{b})}_{\text{elec}}[lN\Lambda,l'N\Lambda']$ is given by eqs 2.2−2.4. As already noted previously,[62] eqs 2.5 and 2.6 show how, through the frame transformation, Rydberg series converging to different rotational states of the core are coupled to one another, $N^{+\prime} = N^+ \pm 1$, ± 2, ± 3, ± 4, ... for $\Lambda \neq 0$ and $N^{+\prime} = N^+ \pm 2$, ± 4, ... when $\Lambda = 0$.

For the high l states, the core−electron interaction is described by the dipolar and quadrupolar terms of the long range multipolar expansion, since the core NO^+ has a permanent dipole and quadrupole

$$V = \sum_{\lambda} (\mu_\lambda P_\lambda(\cos\chi))/r^{\lambda+1}, \quad \lambda = 1, 2 \tag{2.7}$$

where χ is the angle between **r** and the molecular axis. The dipolar $\langle nl|(1/r^2)|n'l'\rangle \langle N^+ m_{N^+} l m_l|\cos\chi|N^{+\prime} m'_{N^+} l' m'_l\rangle$ and quadrupolar $\langle nl|(1/r^3)|n'l'\rangle \langle N^+ m_{N^+} l m_l|P_2(\cos\chi)|N^{+\prime} m'_{N^+} l' m'_l\rangle$ matrix elements are determined as follows. The computation of the angular part is standard.[86] For the radial parts $\langle nl|(1/r^2)|n'l'\rangle$ and $\langle nl|(1/r^3)|n'l'\rangle$, we use exact radial electronic wave functions rather than the simple Bessel function approximation.[87] This was shown[48,66] to be important to get a quantitatively exact value of the integral, in particular for the dipolar interaction.[66] The latter has a long range character and therefore is not well screened by the centrifugal barrier, with the consequence that high l values (l up to about $n/2$) are significantly coupled.

In the presence of the external dc field, the total angular momentum quantum number N is not conserved. Therefore, for the molecular Hamiltonian (2.1), the only conserved quantum number is M, the projection of the total angular momentum **N**. The Stark matrix elements are $\langle nl|r|n'l'\rangle \langle lm_l|\cos\theta|l'm'_l\rangle$, where θ is the angle between **r** and the quantization axis z. The angular part leads to the selection rules $\Delta l = \pm 1$, $\Delta m_l = 0$, and the radial part is analytical[87] for $\Delta n = 0$. The $\Delta n \neq 0$ coupling terms, which are responsible for n mixing and become important above the Inglis−Teller limit, are computed exactly using the same numerical procedure as for the long range dipolar and quadrupolar matrix elements.[48,66]

2.2. Effective Hamiltonian. The low l Rydberg states of NO are known to strongly predissociate,[55] and we use an effective Hamiltonian formalism[68,69] to take into account the coupling to the fragmentation channel. The full effective Hamiltonian, H, in the bound subspace, **Q**, ($I = \mathbf{Q} + P$), is

$$H = \mathbf{Q}H\mathbf{Q} - i\mathbf{Q}\Gamma\mathbf{Q}$$
$$\mathbf{Q}H\mathbf{Q} = \mathbf{Q}(H_{\text{elec}} + H_{\text{rot}} + V + U)\mathbf{Q} \tag{2.8}$$

where $\mathbf{Q}H\mathbf{Q}$ is the real part of the effective Hamiltonian including the interseries coupling and the effect of the external dc field as defined in eq 2.1. We replace the full rate operator $\mathbf{Q}\Gamma\mathbf{Q}$, which describes the predissociation process by its Hermitian part, which amounts to neglecting the level shift of the bound states caused by their coupling to the continuum. We use for the zero-order predissociation widths of the low l states ($l \leq 3$) the same values as those used in refs 61 and 62. Higher l states are assumed to be stable with respect to the predissociation process. In this study we fully diagonalize the effective Hamiltonian and do not treat the predissociation as a perturbation of the bound state dynamics. This was shown to be essential in order to obtain accurate distributions of lifetimes (given by the imaginary part of the complex eigenvalues of the effective Hamitonian) in the case where a large number of quasidegenerate states are coupled to a small number of decay channels.[72,79] In such a case, the rate matrix Γ is of low rank,[88] that is, has a small number of finite eigenvalues (equal to the number of open decay channels) and a much larger number of zero eigenvalues. When the full effective Hamiltonian, $H = \mathbf{Q}H\mathbf{Q} - i\mathbf{Q}\Gamma\mathbf{Q}$ is diagonalized, the intramolecular mixing induced by the real part of the effective Hamiltonian $\mathbf{Q}H\mathbf{Q}$ (interseries coupling and external dc field) leads to a mixing of the fully trapped (zero eigenvalue) and of the prompt eigenstates (finite eigenvalues) of the rate matrix Γ. However, for dense quasibound structures such as high molecular Rydberg states, this mixing is limited by dynamical bottlenecks in phase space and remains incomplete.[48,89] As a result, the individual lifetimes of the Rydberg states follow a bimodal distribution with a very small group (of about 50 states in this case) of promptly decaying states and a much larger group (of about 2500 states) of slowly decaying states, which are responsible for the short- and long-time components of the ZEKE intensity, respectively.[49]

The eigenstates of the full effective Hamiltonian have a biorthogonal character.[69] In such a case, the total decay law $P(t)$ is not a single sum of decaying exponentials but takes the form

$$P(t) = \sum_{s,r}^{N} \langle i|A^\dagger|r^*\rangle\langle r|s\rangle\langle s^*|A|i\rangle \exp(-i(\lambda_s - \lambda_r^*)t/\hbar) \tag{2.9}$$

where A is the transition operator from the intermediate electronic state $|i\rangle$. The decay of $P(t)$ (2.9) is monotonic but can exhibit plateaus. This behavior is typical of overlapping resonances and has already been reported in other contexts.[90,91]

A grouping procedure[48] is used to numerically diagonalize the full effective Hamiltonian. Zero order states with common values of the quantum numbers n, l, N^+, and M (but with different values of the projection quantum numbers m_l and m_{N^+} such that $m_{N^+} + m_l = M$) are grouped together. This grouping procedure typically reduces the size of the basis set from a few tens of thousands to a few thousands. To get a correct description of the effect of the stray field in assisting the interseries coupling, all the l values from 0 to $n - 1$ for each n value are individually included in the basis set and are not grouped together.

2.3. ZEKE Cross Section. The ZEKE intensity is computed both as a function of the delay time, τ, and as a function of the excitation laser frequency for a given strength of the delayed pulsed field used for detection. The formalism used is described in detail in ref 80. Central to ZEKE spectroscopy is the notion of a detection window, which counts all the Rydberg states that can be ionized by the delayed pulsed field. A useful approximation is to write it as a projector on all those bound states that can be ionized for a given strength of the delayed field, F:

$$\Pi \cong \theta((16F/E_n^{\,2}) - 1) - \theta((16F_s/E_n^{\,2}) - 1) \tag{2.10}$$

Here $\theta(x)$ is the unit step function, F (in V/cm) is the external field, F_s is the inevitably present stray field, which causes ionization of the very highest Rydberg states and hence removes them from the detection window, and $E_n = -\text{Ry}/n^2$ is the energy (in cm^{-1}) of the Rydberg states, where Ry is the Rydberg constant. The ZEKE cross section is determined by the expectation value of the detection window Π (eq 2.10) over the ZEKE wave function at the delay time τ, $\text{ZEKE}(\omega, \tau) \equiv \langle\Psi^{(1)}(\tau)|\Pi|\Psi^{(1)}(\tau)\rangle$.[80] The ZEKE wave function $Q|\psi^{(1)}(\tau)\rangle$ is first order in the excitation laser field whose finite width, Γ_l, is included. Therefore, the dynamics which takes place during the laser pulse is fully taken into account in the formalism. The extent to which interseries coupling can occur while the laser is on depends on the strength of the interseries coupling and on the duration of the pulse. The explicit expression of the ZEKE cross section in the biorthogonal basis which diagonalizes the effective Hamiltonian, is[80]

$$\mathrm{ZEKE}(\omega,\tau)=\sum_{n=0}^{N_d}|\langle n|\Psi^{(1)}(\tau)\rangle|^2=\sum_{n=0}^{N_d}\left|\sum_{s=0}^{N}\frac{\exp(-i\lambda_s\tau/\hbar)\langle n|s\rangle\langle s^*|A|i\rangle}{\omega-\lambda_s/\hbar+i\Gamma_l/\hbar}\right|^2 \quad (2.11)$$

where A and $|i\rangle$ have the same meaning as in (2.9), N_d is the number of zero-order states n in the detection window, and N is the dimension of the basis set used to describe the band of quasi-isoenergetic Rydberg states. The λ_s's are the complex eigenvalues that correspond to the biorthogonal states s. For a biorthogonal basis set, the explicit expression for the complex conjugate $\langle\Psi^{(1)}(\tau)|n\rangle$ is

$$\langle\Psi^{(1)}(\tau)|n\rangle=\sum_{r=0}^{N}\frac{\langle i|A^\dagger|r^*\rangle\langle r|n\rangle\exp(i\lambda_r^*\tau/\hbar)}{\omega-\lambda_r^*/\hbar-i\Gamma_l/\hbar} \quad (2.12)$$

The detection operator Π (2.10) typically projects onto a subset of bound states (i.e., those that are in the detection window) and does not commute with the effective Hamiltonian. Therefore, the time evolution of the ZEKE intensity can be nonmonotonic when the pulsed field used for detection is not strong enough to detect the entire subset of quasibound states. In the frequency domain, this noncommutation is responsible for non-Franck−Condon intensities, as has been experimentally observed.[21,92−94]

When the delayed pulsed field used for the detection is strong enough to ionize all the Rydberg states of all the series accessed during the dynamics, that is, when all the quasibound states are detected, the ZEKE cross section takes the form

$$\mathrm{ZEKE}(\omega,\tau)=\sum_{s,r}^{N}\frac{\langle i|A^\dagger|r^*\rangle\langle r|s\rangle\langle s^*|A|i\rangle\exp(-i(\lambda_s-\lambda_r^*)\tau/\hbar)}{(\omega-\lambda_s/\hbar+i\Gamma_l/\hbar)(\omega-\lambda_r^*/\hbar-i\Gamma_l/\hbar)} \quad (2.13)$$

As discussed in ref 80, due to the frequency dependence of the weight, this form is not equivalent to the total decay law $P(t)$ (eq 2.9). It will, however, when plotted as a function of the delay time, τ, exhibit plateaus in the same way as the decay law $P(t)$ (eq 2.9).

3. Computational Results and Discussion

Time- and frequency-resolved ZEKE spectra were computed at different strengths of the external dc field for isoenergetic Rydberg states built on one ($N^+=0$), three ($N^+=0$, 2, 4), and five ($N^+=0-4$) rotational states of NO^+ at an excitation energy about 10 cm^{-1} below the lowest ionization threshold. As discussed in section 2, for the low l states ($l\le 2$), the interseries coupling is included using the MQDT formalism and for the high l states it is included by using a long range multipolar expansion. The MQDT parameters are the same as the ones used in ref 62, which were inferred from previous studies.[55,60] For the long range multipolar expansion, the dipolar constant, μ, of NO^+ is taken from an ab initio computation[95] and is equal to 0.66 Debye (=0.26 au) and the quadrupolar one, Q, is the one determined from ref 96 and is equal to 0.59 au. Recent experimental work suggests that the dipolar interaction, even though weaker than the quadrupolar one, may play a significant role in the dynamics.[59] There is no experimental determination of the permanent dipolar moment of NO^+, and the value of the computed dipolar moment is known to be quite sensitive to the degree of electron correlation and the kind of basis sets used for the computations. Therefore, we have also carried out some computations with a value of the dipolar moment equal to 0.11 au, as reported for more recent ab initio computations,[97,98] in order to check that our results are not significantly modified by using a smaller value of the dipolar moment. We use for the predissociation decay rates the same values as those used in refs 61 and 62, which were inferred from experimental results.[55] All computations were done for $M=0$. The following basis set was used for the five series computation: $N^+=0$, $n=95-107$; $N^+=1$, $n=82-90$; $N^+=2$, $n=67-71$; $N^+=3$, $n=55-57$; $N^+=4$, $n=46-47$. For each n value, all l states are included, which leads to 2693 grouped states (7249 ungrouped). For the one series computation, only those states built on $N^+=0$ are included, which leads to 1313 grouped states (same number ungrouped). For the three series computations, the states built on $N^+=0$, 2, and 4 lead to a total of 1684 grouped states (3476 ungrouped).

Varying the number of Rydberg series included in the basis set allows us to compare the decay kinetics of the ZEKE intensity (i) in the absence of interseries coupling (one series computation including states built on $N^+=0$ only), (ii) in the presence of the low l and of the high l quadrupolar interactions only (for the three series computation, since only Rydberg states converging on $N^+=0$, 2, and 4 are included in the basis), and (iii) in the presence the low l together with both the high l dipolar and quadrupolar interactions (five series computation including states built on $N^+=0$, 1, 2, 3, and 4). To study the synergy between the external dc field and the interseries coupling, we report the ZEKE intensities for two strengths of the external dc field: $F=0.04$ and 0.5 V/cm. In addition, a five-series computation at $F=0.04$ V/cm where only the low l interseries coupling (as parametrized by MQDT) is included, was carried out in order to investigate the role of the long range coupling terms on the decay kinetics of the ZEKE intensity.

In Figure 1, a schematic view of the zero-order position of quasi-isoenergetic Rydberg states in neighboring series is drawn together with the width of the Stark manifold for increasing field strengths. The quantum defect energy shift is shown for the p state only, which is the most shifted state. There are two parameters that must be taken into account to analyze the role of the external dc field on the dynamics. First, the parameter n_μ that gives the field or equivalently the value of n for which the p (or s or d) state is brought into the higher l Stark manifold. This is the parameter discussed in refs 11, 29, 31, 55, and 61, $n_\mu=(2\mu/(3F(\mathrm{au})))^{1/5}$ or equivalently $F_\mu(\mathrm{au})=2\mu/(3n^5)$. Then, there is the parameter n_{IT}, which describes the usual Inglis−Teller (IT) limit[78] where the onset for n mixing within a single series occurs. $n_{IT}=(1/(3F(\mathrm{au}))^{1/5}$, or equivalently $F_{IT}(\mathrm{au})=1/(3n^5)$. In general, $n_\mu<n_{IT}$ and $F_{IT}>F_\mu$, since μ is defined modulo 1.

The parameters n_μ and n_{IT} govern the intraseries mixing. When $n<n_\mu$, no significant l mixing occurs between the state under consideration and the higher l Stark manifold and the lifetime of the state is close to its field-free value. When $n>n_\mu$ and $n<n_{IT}$, good mixing occurs between the fast predissociating low l zero-order states and the higher l states because the field is strong enough to overcome the energy shift caused by the quantum defect. There is intraseries dilution, but the adjacent $n\pm1$ Stark manifolds have not yet bridged. There are still gaps between the levels within a given series, and the interseries coupling is not yet well assisted by the field. Its efficiency still depends on accidental degeneracies. For $n<n_{IT}$, there occurs overlapping of Stark manifolds within a single series. At this point, the occurrence of interseries coupling

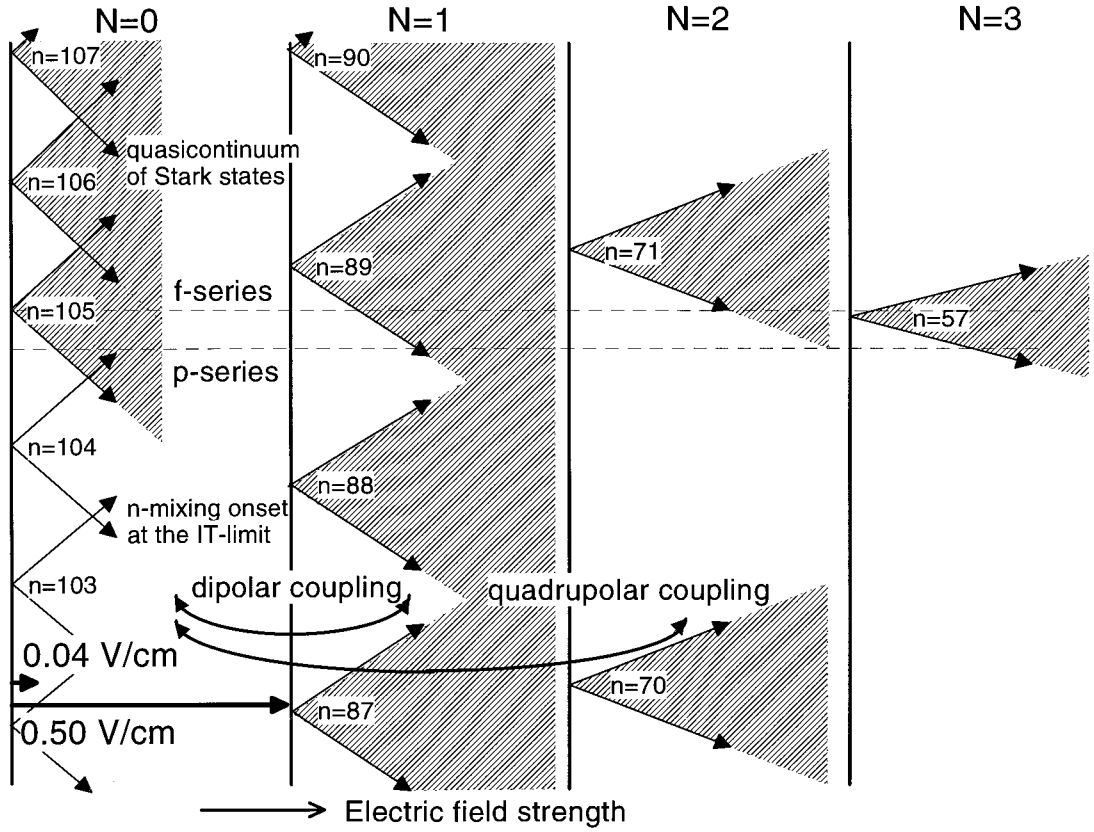

Figure 1. Zero-order positions of quasi-isoenergetic Rydberg states converging on different rotational states of the molecular core as a function of the strength of the external dc field. The width of the Stark manifolds is represented in dashed areas and the zero field position of the p series ($\mu_p = 0.29$) and f series ($\mu_f = 0$) are shown in dashes. The strengths of the two fields used in the computation is also indicated.

TABLE 1: Effect of Interseries Coupling on the Decay Kinetics of the ZEKE Intensity as a Function of the Delay Time for the Initial State $N^+ = 0$, $n = 105$ f at a Field Strength of 0.04 V/cm[a]

	one series	three series	five series
$\tau_{short}/\mu s$	0.13 (98%)	0.16 (54%)	0.38 (75%)
$\tau_{long}/\mu s$	7.5 (2%)	1.19 (46%)	12.2 (23%)

[a] The decay constants τ_{short} and τ_{long} and the relative weights (in %) of the two components are determined from a weighted least-squares fit of the ZEKE intensity to a biexponential form. The three- and the five-series computations include both the short range and the long range core−electron interactions.

reaches its maximum efficiency and ceases to be accidental. In the decay kinetics, the long-time component reaches its maximum value.

3.1. Role of the Interseries Coupling. *One versus five series computations for n =105 f.* Figure 2 and Table 1 illustrate the effect of the interseries coupling on the decay dynamics. In Figure 2, the decay kinetics of the ZEKE intensity of the initial state $N^+ = 0$, $n = 105$ f is plotted as a function of the delay time for a one- and a five-series computation for a strength of the stray field of 0.04 V/cm and a width of the excitation laser of 0.005 cm^{-1}. This laser bandwidth is narrow enough that some interseries dynamics between neighboring series already takes place during the laser pulse. The decay kinetics plotted in Figure 2 is obtained by integrating the computed ZEKE intensity over a range of 0.3 cm^{-1} as a function of the frequency at different delay times (The formalism is discussed in Section 2.3). In this computation, all the quasibound states are detected by the delayed pulsed field and the region of initial excitation is included in the detection window so that the ZEKE intensity decays monotonically as a function of the delay time. An

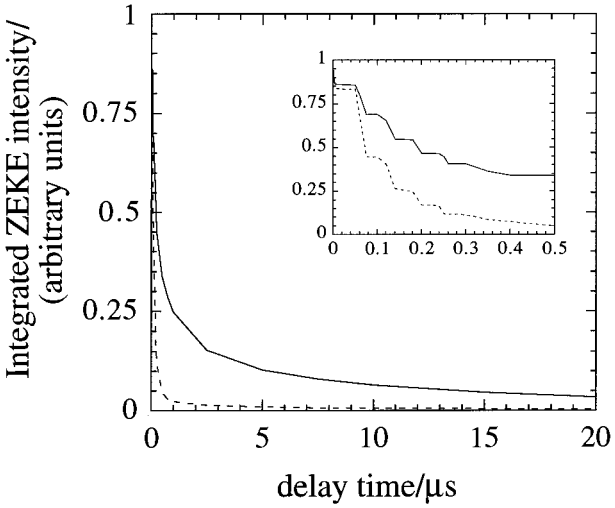

Figure 2. Decay kinetics of the ZEKE intensity as a function of the delay time for a one-series computation (dashes) and for a five-series computation (solid line), including both the short range and the long range interactions. The spectra used to obtain the decay kinetics are computed at a field strength equal to 0.04 V/cm for a width of the excitation laser equal to 0.005 cm^{-1} as in the experiments.[55] Note that at such a high resolution, some interseries dynamics can already occur during the excitation by the laser and this process is taken into account by eq 2.11. The decay kinetics is obtained by integrating the ZEKE intensity over a frequency range of 0.3 cm^{-1}. The intensity at different delay times is normalized to that of $\tau = 0$. The decay constants are reported in Table 1. The decay of the five series computation is clearly biexponential. The short-time behavior is plotted in the insert. The plateaus have a duration equal to the Stark period. The population decays each time the Rydberg electron comes back to low l states, which are the only ones that can predissociate. At longer times, better l mixing is reached and the structure is washed out.

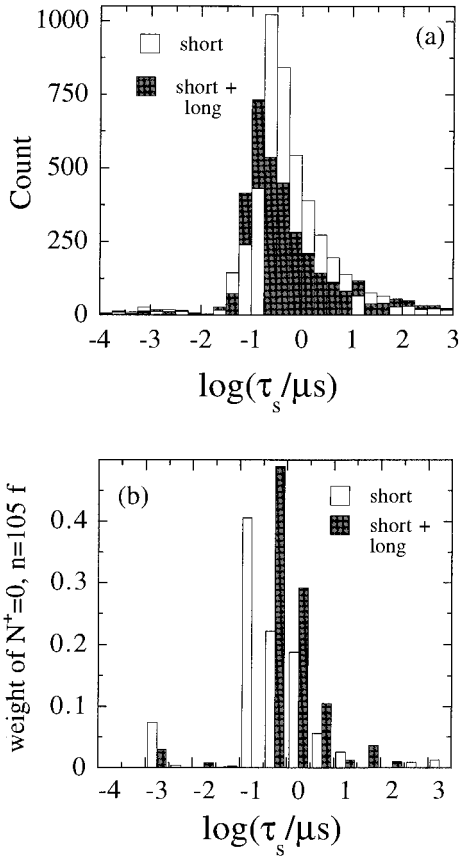

Figure 3. (a) Histogram of the lifetimes (imaginary part of the eigenvalues of the effective Hamiltonian) in microseconds on a logarithmic scale for two five-series computations (2693 states), one including only short range (low *l*) interactions as parametrized by MQDT and the other one including both short range and long range interactions. The legend is as indicated in the figure. The bins with the larger number of states are plotted first on the vertical axis. The very prompt states whose number is equal to the number of open decay channels (≈50) fall in the nanosecond range. The major fraction of the states, which at zero order are not coupled to the fragmentation channels, are delayed. (b) Weights of the initial state $N^+ = 0$, $n = 105$ f on the eigenstates of the two same Hamiltonians as in (a). The histograms are plotted as a function of the lifetimes of the eigenstates (in microseconds, logarithmic scale). For the computation including both short range and long range interactions, the major weights are clearly shifted to eigenstates with longer lifetimes.

analysis of the time dependence of the calculated decay curves shows that these decays are multiexponential. Specifically, the decay of the five-series computation reported in Figure 2 is best fitted by a biexponential decay law (cf. Table 1), with a short range component in the submicrosecond range ($\tau_{\text{short}} = 0.38$ μs) and a long-time component in the tens of microseconds ($\tau_{\text{long}} = 12.2$ μs). On the other hand, the long-time component is almost completely absent from the decay of the one series computation, which takes place in the submicrosecond range. The comparison between the one and the five series decay laws illustrates the fact that interseries dynamics does not quench the long-time component in the decay kinetics but rather enhances it. This is due, as we discuss below (see Figure 3) to the role of the dipolar coupling, which is assisted by the external dc field.

The decay kinetics in the submicrosecond range is plotted in the insert of Figure 2. The length of the plateaus corresponds to the Stark period (=66 ns). The decay resumes each time the Rydberg electron comes in low *l* states where predissociation can occur and is prevented when the Rydberg electron is localized in high *l* states, which results in a plateau in the decay kinetics. Note for comparison that the decay of the one series computation is completed in about three Stark periods.

To enable a quantitative comparison of the different computations, we fitted all the calculated curves to a biexponential form, using a weighted least-squares procedure. Results for the calculations shown in Figure 2 are reported in Table 1, together with the ones resulting from a three series computation. The role of the interseries coupling is evident in lengthening both the short time and the long time decay constants. At this low value of the field, none of the series are above the IT limit and the field is just strong enough for the mixing of the $N^+ = 0$, $n = 105$ d state into the Stark manifold while the p state remains unmixed. As a result, in the one-series computation, the decay constant is slightly shorter than the zero-order predissociation lifetime ($\tau_{0f} = 0.142$ μs). Note that for the multiseries computations, both the short- and a fortiori the long time decay constants are longer than the zero-order predissociation rates.

Role of the Dipolar Interaction. The short and the long decay constants of the decay kinetics resulting from the five-series computation are longer by a factor 2 and 10, respectively, than the ones obtained from the three-series computation. This result shows the particular importance of the dipolar interactions as compared to the quadrupolar interactions. Compared to the one-series computation, the increase of the volume in phase space of significantly coupled isoenergetic states for the five-series computation where the dipolar interactions are included is of about a factor of 2, while the increase of the volume in phase space for the three-series computation is only 30%. To investigate whether the dipolar or the quadrupolar interactions are important predominantly at short range (low *l*) or at long range (high *l*), we have analyzed the distribution of the lifetimes of the individual Rydberg states (defined as the imaginary part of the eigenvalues of the effective Hamiltonian discussed in section 2) and the localization of the prompt and the delayed eigenstates on the zero-order states for the *two* following five-series computations at $F = 0.04$ V/cm: one where only the short range interseries coupling is taken into account and one where both the short range and the long range interseries dipolar and quadrupolar coupling are included. The histograms of the lifetimes (in microseconds, on a logarithmic scale) resulting from the diagonalization of the two five series effective Hamiltonians are plotted in Figure 3a ((shaded) both the short and the long range coupling terms are included; (plain) short range matrix elements only, the bins with the higher weight are plotted first on the vertical axis). As discussed in section 2.2, due to the high density of quasibound states, which are coupled to a small number of open channels, there is a narrow bottleneck for predissociation and the intramolecular redistribution of the predissociation coupling strength induced by the interseries coupling and by the intraseries coupling due to the external dc field is nonuniform.[99] The histograms plotted in Figure 3a are therefore clearly bimodal, with a small group (≈50) of very prompt eigenstates (with a lifetime in the nanosecond range) and a much larger group of delayed states (≈2500), with a lifetime in the microsecond range**.** The inclusion of the long range interaction increases significantly the fraction of lifetimes between 0.1 and 10 μs, with comparatively less very prompt and very delayed eigenstates. This effect is an indication of the better mixing resulting from the inclusion of the long range interaction, which tends to lead to a more uniform distribution of the lifetimes.

The analysis of the weights of the two sets of eigenstates (resulting from the diagonalization of the effective Hamiltonians with and without long range core−electron interactions) on the

TABLE 2: Effect of the Field Strength on the Decay Constants of the ZEKE Intensity as a Function of the Delay Time for the Initial States $N^+ = 0$, $n = 105$ p and f[a]

	$N^+ = 0$ $n = 105$ p	$N^+ = 0$ $n = 105$ f
$F = 0.04$ V/cm		
$\tau_{short}/\mu s$	0.009 (85%)	0.38 (77%)
$\tau_{long}/\mu s$	0.22 (14%)	12.2 (23%)
$F = 0.5$ V/cm		
$\tau_{short}/\mu s$	0.472 (77%)	0.45 (79%)
$\tau_{long}/\mu s$	37.12 (23%)	38.4 (21%)

[a] The ZEKE spectra are computed for a five-series basis set including both short range and long range core−electron interaction.

zero-order states shows that the degree of interseries mixing is increased by a factor of 2 by the long range coupling. The dipolar term, in particular, significantly increases the degree of l mixing between high l states belonging to neighboring series. Between the $N^+ = 0$ and $N^+ = 1$ series, the long range dipolar matrix elements have a strength of about 10^{-4} cm^{-1} up to $l \approx n/2$ due to the long range character of the dipolar interaction.[66] The role of the long range quadrupolar matrix elements, which are localized in low l values, is more limited. (These matrix elements vary between 5×10^{-4} and 5×10^{-5} cm^{-1} between $l = 3$ and $l = 8$. For comparison, the magnitude of the short range matrix elements varies between 5×10^{-2} and 5×10^{-3} cm^{-1}.) As a result of the better l mixing induced both by the dipolar interseries coupling and the intraseries Stark coupling, the zero-order predissociation widths of the low l states are better mixed with the high l states, thereby leading to a larger number of long-living eigenstates with a lifetime between 0.1 and 10 μs.

The occurrence of a larger number of states with lifetimes in the range 0.1−10 μs range would, of course, only lead to different experimental observations at these delay times, if the accessibility of these states remains as good as before. When we analyze the accessibility of these states (Figure 3b), we actually find that it is better than before, since these states better overlap with the initial state. In Figure 3b, the weights of the initial state $N^+ = 0$, $n = 105$ f on the eigenstates of the two effective Hamiltonians (with and without long range interaction) are plotted as a function of the lifetimes of the eigenstates expressed in microseconds (logarithmic scale, same convention as in Figure 3a). The significant weights are clearly shifted to eigenstates with lifetimes between 0.1 and 10 μs when the long range coupling is included. The decay constants of the decay kinetics of the ZEKE intensity resulting from the five-series computation without the long range interseries coupling are 0.25 (weight 93%) and 31.8 μs (weight 7%) to be compared with 0.38 (75%) and 12.2 μs (25%) when the long range interaction is included. So to summarize, the effect of the better mixing is 2-fold. The better mixing leads to a somewhat "less short" short decay constant and a "less long" long decay constant. In addition, the better mixing leads to the better accessibility of the high l states, which represent a large fraction of the total phase space and the weight of the long-time component is larger.

3.2. Role of the Strength of the External Field. Table 2 compares the decay constants of the ZEKE intensity of the two initial states $N^+ = 0$, $n = 105$ p and f at two strengths of the external dc field, $F = 0.04$ and 0.5 V/cm for a five-series basis set including both low l and high l core−electron interactions. For $F = 0.04$ V/cm, $n_{IT} = 133$, which means that all the series included in the basis set are below the IT limit. The interseries mixing, as discussed above in the case of the f state, leads to a short and a long decay time constant that are longer than the ones obtained from the one series computation (which de facto neglects the interseries coupling). The p state, whose zeroth-order lifetime equals 3.8 ns ($\Gamma_{0p} = 1600$ cm^{-1}), decays faster than the f state ($\tau_{0f} = 142$ ns) with a short time decay constant of about three zero-order lifetimes and a long time decay constant 50 times longer than τ_{0p}. For $F = 0.04$ V/cm, the p state is not yet merged into the higher l manifold by the external field and the Stark period is much larger than both its zero-order predissociation lifetime and the short range interseries coupling. Note that at this field strength, where all the series are below the IT limit, we are still in the regime of accidental degeneracies. Therefore, the details of decay kinetics of the ZEKE intensity vary from one initial state to the next. However, in the multiseries case, all the initial states investigated exhibit a short-time component in the submicrosecond range and a long-time component with a decay constant at least 10 times larger. The long-time component is almost absent from the one series computation and is a manifestation of the effects of the interseries coupling, in particular of the long range dipolar term.

At $F = 0.5$ V/cm, the Stark period is comparable to the period of the short range coupling and to the zero-order lifetime of the fast predissociating p states. Both the states of the $N^+ = 0$ and the $N^+ = 1$ series are above the IT limit ($n_{IT} = 80$) so that due to n mixing, these two series have a uniform density of states. In this case, the interseries coupling is well assisted by the external dc field and the states up to $N^+ = 2$ are well mixed. As a result, the p and the f states have the same decay kinetics and can be fitted to a biexponential form with the same parameters. The short decay constant is ≈0.45 μs with a weight of ∼80%, and long one is 38 μs with a weight of ≈20%. The fact that the p and the f states decay similarly is consistent with the fact that the mixing has reached its maximal efficiency, with the enhancement of the decay constants being particularly important for the long-time component, which now extends in the tens of microseconds range. This conclusion is also supported by the analysis of the degree of mixing of the zero-order states brought by the diagonalization of the effective Hamiltonian. Strictly speaking, in such a case, one cannot excite a p or an f state individually but only a superposition of zero-order hydrogenic states. The situation described above resembles very closely, in our view, the situation that will occur in an actual ZEKE experiment (n about 200, F about 0.025 V/cm). Our calculations predict that under actual ZEKE conditions the decay of the "ZEKE Rydberg states" will be approximately biexponential, with a short time decay rate of ≈1 μs and a long time one of ≥40 μs. As suggested by previous studies,[48] the prompt decay constant scales approximately as n^3, since it corresponds to the decay rates that are very little affected by the nonuniform inter- and intraseries mixing induced by the core−electron interactions and the external dc field, respectively. The scaling of the long time decay, which depends on the efficiency of the interseries coupling, is expected to range between n^4 and n.[5]

The long-time component of the decay kinetics is not significantly affected by using a smaller value of the dipolar constant, $\mu_{NO^+} = 0.11$ au.[97,98] At $F = 0.04$ V/cm, for this value of the dipolar constant, the decay kinetics of the initial state $N^+ = 0$, $n = 105$ f computed for a five-series basis set has a short-time component with a decay constant of 0.36 μs and a weight of 87%, while the long time component has a decay constant of 20.7 μs with a weight of 13%. Since a smaller value of the dipole moment leads to a slightly less good mixing, this result is intermediate between the decay kinetics (reported in Table 2) obtained for the higher value of the dipolar moment, $\mu_{NO^+} = 0.26$ au, and that discussed in section 3.1, obtained for

the computation where the long range interseries coupling among high l states is neglected. At this same field strength of 0.04 V/cm, the decay of the $N^+ = 0$, $n = 105$ p state, whose zero-order predissociation rate is much larger than the strength of the long range dipolar coupling, is not affected by using a smaller dipolar constant. At $F = 0.5$ V/cm, where the lowest two series are above the IT limit and the interseries coupling is well assisted by the external dc field, the decay laws of both the $n = 105$ p and f states are almost not affected by reducing the value of the dipolar constant to 0.11 au.

3.3. Role of the Localization of the Initial Excitation. At a given field strength, the amount of interseries population transfer very much depends on the localization of the initial state. When the initial state is localized in the lowest N^+ series, this transfer is less extensive than when it is localized on a higher state of the core. The reason is that in the former case, the transfer occurs from a denser to a sparser series, a process which is unfavorable. In addition, in the case of a predissociation process, Rydberg states built on higher rotational states of the core predissociate faster, which means that the population transferred does not accumulate in the series corresponding to excited states of the core. Another important factor is the strength of the external dc field with respect to the strengths of the interseries coupling and the predissociation process as discussed above. At $F = 0.5$ V/cm, the Stark period is of the order of a few nanoseconds and comparable to the period of the short range interseries coupling and the predissociation lifetimes of the p and the d states. The transfer to high l competes with or precedes the interseries coupling. In addition, the population that is transferred to low l states of other series quickly decays. For an initial state ($n = 105$) localized in the $N^+ = 0$ series, the population trapped at long time in the high l states of higher series is about 5%. (At $F = 0.04$ V/cm, where none of the series is above the IT limit, this amount is about 1%).

The situation is quite different when the initial state is localized in the $N^+ = 2$ series ($n = 70$), which at $F = 0.5$ V/cm is the first series below the IT limit. The coupling from this sparse series to the much better mixed and denser lower series $N^+ = 1$ and 0 is very much favored, which results in a population transfer to these lower series of about 15% while the amount of population transferred to the higher series ($N^+ = 3$ and 4) is negligible. For an initial state $N^+ = 2$, $n = 70$ f, the short component of the decay kinetics has a decay constant of 0.2 μs (weight 88.2%), while the decay constant of the long-time component is 47.9 μs (weight 11.2%). The lower N^+ series predissociate slower at zero order, since the principal quantum numbers are higher and therefore population can accumulate longer. As before, the interseries population transfer occurs at short times.

On a submicrosecond time scale and at a given delay time, the ZEKE intensity varies extensively as a function of the excitation frequency. In Figure 4, the ZEKE intensities for two different detection windows, localized in the $N^+ = 2$ (dashes) and in the $N = 0$ and 1 (solid line) series, respectively, are plotted as a function of the excitation frequency for delay times equal to 0.005, 0.075, and 2.5 μs. The spectra have been computed for the same initial state $N^+ = 2$, $n = 70$ f whose decay kinetics was discussed above, i.e., localized in the first series that is not above the IT limit, at a field strength of 0.5 V/cm. At this field strength, the zero-order states and in particular the ones of the two lowest series, which are above the IT limit, are pretty well mixed, which precludes a definite assignment of the structures seen in Figure 4. However, the

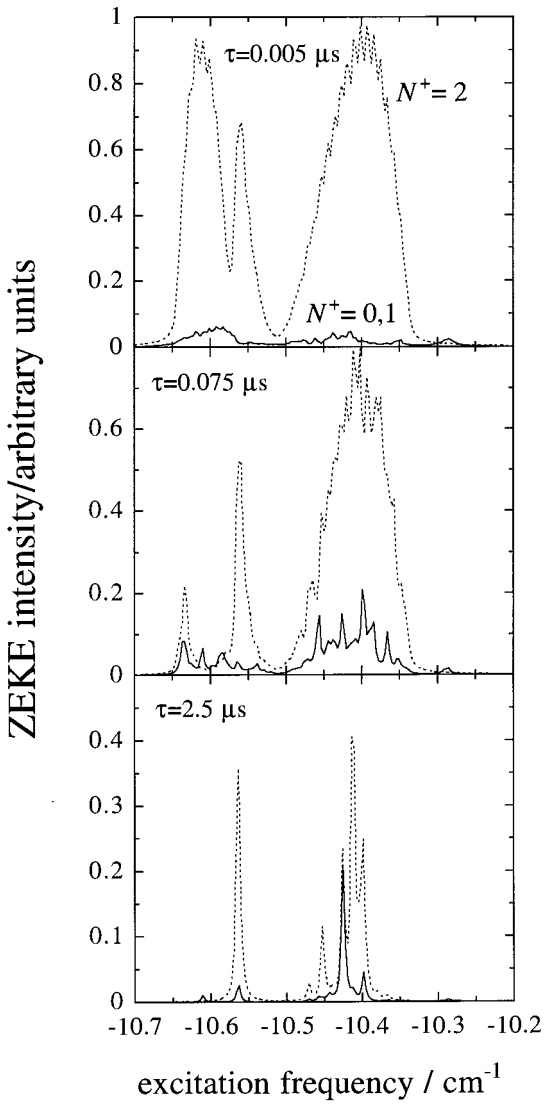

Figure 4. ZEKE spectra as a function of the excitation frequency for three different delay times as indicated. The spectra are computed for the initial state $N^+ = 2$, $n = 70$ f at $F = 0.5$ V/cm with the five-series basis set including both short and long range core−electron interactions for two detection windows, one that corresponds to the states of the series initially excited (dashes) and one that corresponds to the states of the two lower series $N^+ = 0$ and 1 (solid). At a delay time shorter than the Stark period ($2\pi/(3nF) = 7.4$ ns), only a small amount of population transfer to the lower series has occurred (upper panel). In the intermediate panel, the delay time is about 10 Stark periods and the interseries population transfer is significant. For longer delay times (lower panel), the integrated fraction of the remaining total population ($\approx$10%) in each series is about constant. However, as a function of the excitation frequency, the relative fraction of the population in the different series still varies in a nonmonotonic way. Note how the spectra are sharpening as a function of the delay time due to the decay of the prompt eigenstates.

positions of the lowest peaks (between −10.7 and −10.6) can be correlated to the zero field position (including quantum defect) of the low l states (in particular the s state) of $N^+ = 2$, $n = 70$; $N^+ = 1$, $n = 87$; and $N^+ = 0$, $n = 102$, which are strongly mixed through the short range interactions. The peak around −10.4 cm^{-1} corresponds to the high l manifolds of the same states. The fast oscillations seen in the upper panel are of the order of the Stark spacing $3nF$. In the intermediate panel where the delay time corresponds to about 10 Stark periods for the $N^+ = 0$ states, the population in the lowest series $N^+ = 0$ and 1 is already more uniform. In the bottom panel, the

remaining integrated intensity is only about 10% of the initial one. The prompt states have decayed and the sharp peaks are due to very long-living Rydberg states.

4. Concluding Remarks

The structure of phase space for a predissociation process at excitation energies below the lowest ionization threshold as encountered in this analysis of the Rydberg states of NO is quite different from the one previously investigated for Na_2. Since the low l states of each series predissociate, there are as many bottlenecks for fragmentation as there are coupled series. This opens up the question of if, for a molecule like NO, interseries coupling assists the lifetime enhancement of the Rydberg states (as was the case in Na_2) or is a mechanism that leads to the rapid decay of the existing Rydberg population.

To investigate this question, we have computed the ZEKE spectra and their decay kinetics for a one series and different multiseries basis sets, which enable us to get more insight on the relative importance of the different processes affecting the dynamics: predissociation of the molecular core, short range and long range interseries coupling, and the effect of the external dc field. We find that the decay kinetics of the ZEKE intensity exhibits two time scales and that in this case, where all series are coupled to the fragmentation channels through a low l bottleneck, the predissociation process does not quench the long-time component in the decay kinetics.

The bottlenecks lead to a bimodal distribution of the individual decay rates with a small group of promptly decaying states and a much larger group of delayed states. The interplay between the external dc field and the interseries coupling controls the degree of mixing of the zero order states. The prompt states, which predissociate on a submicrosecond time scale are mainly localized in low l zero-order states of each series, which are predominantly mixed by the short range core−electron interactions. The delayed states are localized mainly in the high l states. The long range interseries coupling among high l states belonging to neighboring series, even though weaker than the short range coupling, plays an important role in the dynamics. Through the long range interseries coupling acting in synergy with intraseries coupling induced by the external dc field, there is a better mixing between low and high l states, which results in a lengthening of the very short lifetimes and a shortening of the very long ones.

For strength of the external dc field where all the series are below the IT limit, one is in the regime of accidental resonances and, within a given range of excitation energies, there can be variations from one initial state to the next; the relative weights of the short- and the long-time component of the decay kinetics and the values of the decay constants depend on the localization of the initial state. For stronger external dc fields, where several series are above the IT limit, the efficiency of the interseries is maximal, due to the more uniform density of states within each Rydberg series. Then, the decay kinetics does not depend on the localization of the initial state. The bottleneck between the low and high l states is made wider by the synergy between the long range interseries coupling and the external dc field. As a result, the weight of the long-living states in the decay dynamics is enlarged.

Our computations lead to a number of interesting predictions, which can be verified by experiment, such as the decay constant and the relative weight of the long-time component, the plateaus in the decay kinetics at short time, and the very rich structure of the ZEKE spectra, which when only a subset of states is detected by the delayed pulse field, varies in a nonmonotonic way as a function of the delay time. For the latter, the recent high resolution work of Merkt et al.[100] is a very promising direction.

Acknowledgment. We are delighted to dedicate this paper to Professor R. D. Levine on the occasion of his 60th birthday. F. Remacle deeply thanks Professor R. D. Levine for being a wonderful teacher and for his profound and stimulating scientific insight and vision. The work of M. J. J. Vrakking is part of the research program of the "Stichting voor Fundamenteel Onderzoek der Materie", which is financially supported by the "Nederlandse organisatie voor Wetenschappelijk Onderzoek". The work of F. Remacle is supported by the "Fonds de la Recherche Fondamentale Collective". The computational work is supported by SFB377. We thank the referee for having drawn our attention to a recent computed value for the dipolar moment of NO^+ and Dr. D. Dehareng for helpful discussions and her determination of the dipolar moment of NO^+.

References and Notes

(1) Müller-Dethlefs, K.; Schlag, E. W. *Annu. Rev. Phys. Chem.* **1991**, *42*, 109.
(2) Zhu, L.; Johnson, P. *J. Chem. Phys.* **1991**, *94*, 5769.
(3) Zhang, X.; Smith, J. M.; Knee, J. L. *J. Chem. Phys.* **1993**, *99*, 3133.
(4) Merkt, F.; Softley, T. P. *Int. Rev. Phys. Chem.* **1993**, *12*, 205.
(5) Müller-Dethlefs, K.; Schlag, E. W.; Grant, E. R.; Wang, K.; McKoy, V. *Adv. Chem. Phys.* **1995**, *90*, 1.
(6) Wang, K.; McKoy, V. *Annu. Rev. Phys. Chem.* **1995**, *46*, 275.
(7) Schlag, E. W. *ZEKE Spectroscopy*; Cambridge University Press: Cambridge, 1998.
(8) Schlag, E. W.; Levine, R. D. *Comments At. Mol. Phys.* **1996**, *33*, 159.
(9) Levine, R. D. *Adv. Chem. Phys.* **1997**, *101*, 625.
(10) Schlag, E. W. *Adv. Chem. Phys.* **1997**, *101*, 607.
(11) Merkt, F. *Annu. Rev. Phys. Chem.* **1997**, *48*, 675.
(12) Reiser, G.; Habenicht, W.; Müller-Dethlefs, K.; Schlag, E. W. *Chem. Phys. Lett.* **1988**, *152*, 119.
(13) Vrakking, M. J. J.; Lee, Y. T. *J. Chem. Phys.* **1995**, *102*, 8833.
(14) Mühlpfordt, A.; Even, U. *J. Chem. Phys.* **1995**, *103*, 4427.
(15) Merkt, F.; Zare, R. N. *J. Chem. Phys.* **1994**, *101*, 3495.
(16) Grant, E. R. In *High-Resolution Laser Photoionization and Photoelectron Studies*; Powis, I.; Baer, T., Ng, C. Y., Ed.; Wiley: New York, 1995.
(17) Merkt, F.; Mackenzie, S. R.; Softley, T. P. *J. Chem. Phys.* **1995**, *103*, 4509.
(18) Vrakking, M. J.; Fischer, I.; Villeneuve, D. M.; Stolow, A. *J. Chem. Phys.* **1995**, *103*, 4538.
(19) Neuhauser, R. G.; Siglow, K.; Neusser, H. J. *J. Chem. Phys.* **1997**, *106*, 896.
(20) Wales, N. P.; Buma, W. J.; Lange, C. A. d.; Lefebvre-Brion, H. *J. Chem. Phys.* **1996**, *105*, 5702.
(21) Matsui, H.; Behm, J. M.; Grant, E. R. *J. Phys. Chem.* **1997**, *101*, 6717.
(22) Held, A.; Baranov, L. Y.; Selzle, H. L.; Schlag, E. W. *J. Chem. Phys.* **1997**, *106*, 6848.
(23) Ivanov, M. Y.; Stolow, A. *Chem. Phys. Lett.* **1997**, *265*, 231.
(24) Held, A.; Baranov, L. Y.; Selzle, H. L.; Schlag, E. W. *Chem. Phys. Lett.* **1997**, *267*, 318.
(25) Bordas, C.; Brevet, P. F.; Broyer, M.; Chevaleyre, J.; Labastie, P.; Perrot, J. P. *Phys. Rev. Lett.* **1988**, *60*, 917.
(26) Chupka, W. A. *J. Chem. Phys.* **1993**, *98*, 4520.
(27) Chupka, W. A. *J. Chem. Phys.* **1993**, *99*, 5800.
(28) Mahon, C. R.; Janik, G. R.; Gallagher, T. F. *Phys. Rev. A* **1990**, *41*, 3746.
(29) Merkt, F.; Fielding, H. H.; Softley, T. P. *Chem. Phys. Lett.* **1993**, *202*, 153.
(30) Rabani, E.; Levine, R. D.; Mühlpfordt, A.; Even, U. *J. Chem. Phys.* **1995**, *102*, 1619.
(31) Rabani, E.; Baranov, L. Y.; Levine, R. D.; Even, U. *Chem. Phys. Lett.* **1994**, *221*, 473.
(32) Bixon, M.; Jortner, J. *J. Phys. Chem.* **1995**, *99*, 7466.
(33) Held, A.; Selzle, H. L.; Schlag, E. W. *J. Phys. Chem.* **1996**, *100*, 15314.
(34) Remacle, F.; Levine, R. D.; Schlag, E. W.; Selzle, H. L.; Held, A. *J. Phys. Chem.* **1996**, *100*, 15320.
(35) Bellomo, P.; Farrelly, D.; Uzer, T. *J. Phys. Chem.* **1997**, *101*, 8902.

(36) Jones, R. R.; Fu, P.; Gallagher, T. F. *J. Chem. Phys.* **1997**, *106*, 3578.
(37) Vrakking, M. J. J. *J. Phys. Chem.* **1997**, *101*, 6761.
(38) Merkt, F. *J. Chem. Phys.* **1994**, *100*, 2623.
(39) Palm, H.; Merkt, F. *Chem. Phys. Lett.* **1997**, *270*, 1.
(40) Dorofeev, D. L.; Zon, B. A. *J. Chem. Phys.* **1997**, *106*, 9609.
(41) Bellomo, P.; Farrelly, D.; Uzer, T. *J. Chem. Phys.* **1997**, *107*, 2499.
(42) Martin, J. D. D.; Hepburn, J. W.; Alcaraz, C. *J. Phys. Chem.* **1997**, *101*, 6728.
(43) Mühlpfordt, A.; Even, U.; Rabani, E.; Levine, R. D. *Phys. Rev. A* **1995**, *51*, 3922.
(44) Palm, H.; Signorell, R.; Merkt, F. *Philos. Trans. R. Soc. London, Ser. A* **1997**, *325*, 1551.
(45) Bahatt, D.; Even, U.; Levine, R. D. *J. Chem. Phys.* **1993**, *98*, 1744.
(46) Even, U.; Levine, R. D.; Bersohn, R. *J. Phys. Chem.* **1994**, *98*, 3472.
(47) Even, U.; Ben-Nun, M.; Levine, R. D. *Chem. Phys. Lett.* **1993**, *210*, 416.
(48) Remacle, F.; Levine, R. D. *J. Chem. Phys.* **1996**, *105*, 4649.
(49) Remacle, F.; Levine, R. D. *J. Chem. Phys.* **1997**, *107*, 3392.
(50) Lefebvre-Brion, H. *Chem. Phys. Lett.* **1997**, *268*, 318.
(51) Jortner, J.; Bixon, M. *J. Chem. Phys.* **1994**, *102*, 5636.
(52) Rabani, E.; Levine, R. D.; Even, U. *J. Phys. Chem.* **1994**, *98*, 8834.
(53) Pratt, S. T. *J. Chem. Phys.* **1993**, *98*, 9241.
(54) Kong, W.; Rodgers, D.; Hepburn, J. W. *J. Chem. Phys.* **1993**, *98*, 8571.
(55) Vrakking, M. J. J.; Lee, Y. T. *J. Chem. Phys.* **1995**, *102*, 8818.
(56) Sato, S.; Kimura, K. *J. Chem. Phys.* **1997**, *107*, 3376.
(57) Park, H.; Leahy, D. J.; Zare, R. N. *Phys. Rev. Lett.* **1996**, *76*, 1591.
(58) Park, H.; Zare, R. N. *J. Chem. Phys.* **1997**, *106*, 2239.
(59) Pratt, S. T. *J. Chem. Phys.* **1998**, *108*, 7131.
(60) Fredin, S.; Gauyacq, D.; Horani, M.; Jungen, C.; Lefevre, G. *Mol. Phys.* **1987**, *60*, 825.
(61) Bixon, M.; Jortner, J. *J. Chem. Phys.* **1996**, *105*, 1363.
(62) Vrakking, M. J. *J. Chem. Phys.* **1996**, *106*, 7336.
(63) Fano, U. *Phys. Rev. A* **1970**, *2*, 353.
(64) Green, C. H.; Jungen, C. *Adv. At. Mol. Phys.* **1985**, *21*, 51.
(65) *Molecular Applications of Quantum Defect Theory*; Jungen, C., Ed.; Institute of Physics: Bristol, 1996.
(66) Baranov, L. Y.; Remacle, F.; Levine, R. D. *Phys. Rev.* **1996**, *A54*, 4789.
(67) Bixon, M.; Jortner, J. *Mol. Phys.* **1996**, *89*, 371.
(68) Feshbach, H. *Ann. Phys. (New York)* **1962**, *19*, 287.
(69) Levine, R. D. *Quantum Mechanics of Molecular Rate Processes*; Oxford University Press: Oxford, 1969.
(70) Ernst, W. E.; Softley, T. P.; Zare, R. N. *Phys. Rev. A* **1988**, *37*, 4172.
(71) Remacle, F.; Levine, R. D. *Phys. Lett.* **1993**, *A173*, 284.
(72) Remacle, F.; Levine, R. D. *J. Chem. Phys.* **1996**, *104*, 1399.
(73) Harmin, D. A. *Phys. Rev. A* **1981**, *24*, 2491.
(74) Sakimoto, K. *J. Phys. B* **1989**, *22*, 2727.
(75) Brevet, P. F.; Bordas, C.; Broyer, M.; Jalbert, G.; Labastie, P. *J. Phys. II* **1991**, *1*, 875.
(76) Softley, T. P.; Hudson, A. J.; Watson, R. *J. Chem. Phys.* **1997**, *106*, 1041.
(77) Remacle, F.; Even, U.; Levine, R. D. *J. Phys. Chem.* **1996**, *100*, 19735.
(78) Gallagher, T. F. *Rydberg Atoms*; Cambridge University Press: Cambridge, 1994.
(79) Remacle, F.; Levine, R. D. *J. Phys. Chem.* **1996**, *100*, 7962.
(80) Remacle, F.; Levine, R. D. *J. Chem. Phys.* **1997**, *107*, 3382.
(81) Lefebvre-Brion, H.; Field, R. W. *Perturbations in the Spectra of Diatomic Molecules*; Academic Press: New York, 1986.
(82) Remacle, F.; Levine, R. D. *Int. J. Quantum Chem.* **1998**, *67*, 85.
(83) Herzberg, G.; Jungen, C. *J. Mol. Spectrosc.* **1972**, *41*, 425.
(84) Giusti-Suzor, A.; Jungen, C. *J. Chem. Phys.* **1984**, *80*, 986.
(85) Bordas, C.; Helm, H. *Phys. Rev. A* **1992**, *45*, 387.
(86) Arthurs, A. M.; Dalgarno, A. *Proc. R. Soc. London* **1960**, *A256*, 540.
(87) Bethe, H. A.; Salpeter, E. E. *Quantum Mechanics of One- and Two-Electron Atoms*; Plenum-Rosetta: New York, 1977.
(88) Remacle, F.; Munster, M.; Pavlov-Verevkin, V. B.; Desouter-Lecomte, M. *Phys. Lett.* **1990**, *A145*, 265.
(89) Remacle, F.; Levine, R. D. *ACH, Model in Chemistry* **1997**, *134*, 619.
(90) Nordholm, S.; Rice, S. A. *J. Chem. Phys.* **1975**, *62*, 157.
(91) Remacle, F.; Desouter-Lecomte, M.; Lorquet, J. C. *J. Chem. Phys.* **1989**, *91*, 4155.
(92) Nemeth, G. I.; Ungar, H.; Yeretzian, C.; Selzle, H. L.; Schlag, E. W. *Chem. Phys. Lett.* **1994**, *228*, 1.
(93) Signorell, R.; Wüest, A.; Merkt, F. *J. Chem. Phys.* in press.
(94) Grebner, T. L.; Unold, P. v.; Neusser, H. J. *J. Phys. Chem.* **1997**, *101*, 158.
(95) Jungen, C.; Lefebvre-Brion, H. *J. Mol. Spectrosc.* **1970**, *33*, 520.
(96) Jungen, C.; Miescher, E. *Can. J. Phys.* **1969**, *47*, 1769.
(97) Fehér, M.; Martin, P. A. *Chem. Phys. Lett.* **1993**, *215*, 565.
(98) This value is in agreement with a recent study[97] and with ab initio unpublished computations of Dr. D. Dehareng who reported to us a value of 0.1176 au for a CASSCF computation (CAS (10,10)/cc-pVQZ) with ($1\sigma^*$, $4\pi^*$) for the virtual orbitals and 0.1069 for the same level of CASSCF computation but with ($3\sigma^*$, $2\pi^*$) for the virtual orbitals. For comparison, the RHF/6-31G** value is 0.2734 au.
(99) Note that this nonuniform dilution is also the case but to a less extent for the one series computation, where the only operative mixing is the l and n mixing due to the external dc field.[48,66.]
(100) Merkt, F.; Schmutz, H. *J. Chem. Phys.* **1998**, *108*, 10033.